



ORIGINAL ARTICLE

Insights into methyl orange adsorption behavior on a cadmium zeolitic-imidazolate framework Cd-ZIF-8: A joint experimental and theoretical study



Bouchra Ba Mohammed ^a, Hassane Lgaz ^{b,*}, Awad A. Alrashdi ^c, Khalid Yamni ^a, Najib Tijani ^a, Younes Dehmani ^d, Hicham El Hamdani ^e, Ill-Min Chung ^{b,*}

^a *Laboratory of Chemistry of Materials and Biotechnology of Natural Products, (E.M.M.P.) Moulay Ismail University, Faculty of Sciences of Meknes, Meknes, Morocco*

^b *Department of Crop Science, College of Sanghur Life Science, Konkuk University, Seoul 05029, South Korea*

^c *Chemistry Department, Umm Al-Qura University, Al-Qunfudah University College, Saudi Arabia*

^d *Laboratory of Chemistry and Biology Applied to the Environment, Moulay Ismail University, Faculty of Sciences of Meknes, Meknes, Morocco*

^e *Métallation, Complexes Moléculaires et Applications (MCMA), Université Moulay Ismail, Faculté des Sciences de Meknès, Morocco*

Received 8 July 2020; accepted 1 November 2020

Available online 10 November 2020

KEYWORDS

Adsorption;
Organic pollutants;
Cadmium-Imidazolate
Framework;
DFT;
Methyl orange

Abstract Dyeing wastewater from textile industries is often contaminated with chemical pollutants, which causes severe water pollution problems that are challenging to treat. Recently, Zeolitic imidazolate frameworks (ZIFs) have attracted extensive research interest due to their potential applications in the removal of pollutants from wastewater. Herein, a Cd-zeolitic-imidazolate framework (Cd-ZIF-8) was synthesized and used as an adsorbent for the removal of methyl orange (MO) at different operating conditions. The prepared adsorbent was characterized using a variety of techniques, including X-ray diffraction (XRD), the Brunauer Emmett Teller (BET) method, FT-IR and scanning electron microscope (SEM). Its stability after adsorption was confirmed by XRD and pH tests. The effects of different variables, such as adsorbent dose, initial concentration, pH and temperature, were investigated to optimize the adsorption process. Adsorption parameters were determined by applying Langmuir and Freundlich models, and good fitting was observed for the Langmuir isotherm. Maximum MO adsorption capacities on Cd-ZIF-8 were 93.24 and 145.41 mg g⁻¹ at 30° and 50°, respectively. Possible controlling mechanism and the potential rate-limiting steps were analyzed using Lagergren's pseudo-first-order and pseudo-second-order

* Corresponding authors.

E-mail addresses: hlgaz@konkuk.ac.kr (H. Lgaz), imcim@konkuk.ac.kr (I.-M. Chung).

Peer review under responsibility of King Saud University.



Production and hosting by Elsevier

models, and the data were found to follow the pseudo-second-order equation. The prepared material was found to have good stability after the adsorption with no release of Cd ions over a wide range of pH. For a further explanation of the adsorption mechanism, interactions of MO molecules with the Cd and organic linkers of ZIF-8 were investigated using Density Functional Theory (DFT) cluster calculations.

© 2020 The Authors. Published by Elsevier B.V. on behalf of King Saud University. This is an open access article under the CC BY-NC-ND license (<http://creativecommons.org/licenses/by-nc-nd/4.0/>).

1. Introduction

Synthetic dyes are notoriously problematic chemical pollutants. These industrial discharges, which are non-biodegradable, are highly toxic to aerobic and aquatic life and can degrade into compounds that exhibit carcinogenic, mutagenic and neurotoxicity effects (Gupta and Khatri, 2019; Jadhav et al., 2019; Zhou et al., 2019). Furthermore, they can significantly prevent light penetration and, thus hinder photosynthesis in aquatic plants (Hou et al., 2020). The inappropriate disposal of a large amount of these harmful dyes does not only result in significant environmental pollution but also in substantial disposal investments, which make the dyeing industry one of the most polluting industries on the planet (Förstner, 2012). Methyl orange (MO), which is widely used in several industries such as food, paper, printing, leather and textile, belongs to the azo dye group; it is detrimental to the environment and thought to be toxic to aquatic life (Alqaragully, 2014; El-Gamal et al., 2015; Mokhtari et al., 2016). Furthermore, acute exposure to methyl orange is known to cause tissue necrosis, quadriplegia, jaundice, cyanosis, shock, vomiting, and increasing heart rate in humans (Darwish et al., 2019).

In such a situation, and given the limited aquatic resources, and the huge demand for safe water, a very large number of technologies such as nanofiltration, adsorption, coagulation/flocculation, electrolysis, electro-Fenton, oxidation, reverse osmosis, etc. have been developed for purification and refining of water (Pavithra and Jaikumar, 2019). As some of these techniques have proved low efficiency, time-consuming, complex, expensive, attention has turned to the use of the adsorption as an effective, simple, and low-cost alternative method (Gupta and Subas, 2009).

Nowadays, several kinds of materials including carbon nanotubes (CNTs), polymeric materials, oxides, and zeolites, etc. are used as adsorbents for wastewater treatment (Bulgariu et al., 2019; Katheresan et al., 2018; Q. Liu et al., 2020; Siyal et al., 2018). In the past two decades, the use of Metal-Organic Frameworks (MOFs) in a wide range of fields such as sensors, molecular storage, gas/heavy metal adsorption, catalysis has gained a significant research interest (Hani Nasser Abdelhamid, H.N. Abdelhamid, 2020; Farrusseng et al., 2009; Férey, 2008; Yaghi et al., 2003). Their structural diversities, tuneable topological pores, high surface areas, and specific functions make these materials a promising candidate for application in many fields including water and air purification (Chueh et al., 2019; Gao et al., 2020; Konnerth et al., 2020; Lee et al., 2019; Liao et al., 2020, 2018; Wu et al., 2020). A successful application of these materials for removal of hazardous compounds such as dyes, polycyclic aromatic hydrocarbons (PAHs), and phenols was described

recently (Abdel-Magied et al., 2019; S. Li et al., 2016; Doherty et al., 2012). Mainly, Zeolitic Imidazolate Frameworks (ZIFs), which are types of MOFs, are of tremendous importance as these materials have a tuneable zeotype topology with a high thermal/chemical stability, a high surface area, and strong adsorption capacity, among others (Y. Li et al., 2016; Phuong et al., 2016).

These excellent physicochemical properties make ZIFs excellent adsorbents for capturing contaminants/gases ranging from small to large toxic molecules from water (Jampa et al., 2020; Konno et al., 2020; J. Li et al., 2018; Wang et al., 2019; Zhu et al., 2017). In this regard, ZIF-8, which has a high surface area, is among the most frequently studied ZIF materials. In ZIF-8, tetrahedrally coordinated zinc ions are bridged by 2-methylimidazole (2-mIm) through its nitrogen atoms. The stability of these porous crystals for water makes them highly attractive materials for repeated adsorptive removal in water (Chin et al., 2018). Recently, it was reported that various modified and unmodified ZIFs materials were successfully used as adsorbents for the elimination of heavy metal and organic contaminants like dyes from wastewater (Huang et al., 2018; Li et al., 2019; T. Li et al., 2018). Many studies are reporting the efficacy of ZIF-8 in the degradation of organic dyes such as rhodamine 6G, triiodide, methylene blue as well as benzotriazoles and phthalic acid, As(III), etc. (Abdelhamid et al., 2017; Chin et al., 2018; Jampa et al., 2020; Konno et al., 2020; Nasser Abdelhamid and Zou, 2018). For instance, Chin et al. reported that nanosized ZIF-8 displays great potential for the adsorption and photodegradation of Rhodamine B (Chin et al., 2018), while it showed a low adsorption capacity for methyl orange (Ding et al., 2017; Y. Li et al., 2016; Zhang et al., 2020).

On the other hand, many computational methods have proven to be a powerful tool in understanding and explaining the adsorption mechanism in various ZIFs (Dong et al., 2019; Wang et al., 2020). In this context, useful insights into the interactions between ZIFs and adsorbates can be obtained by DFT calculations. However, in the case of ZIF-8, there are not many studies combining molecular simulations and adsorption experiments. In the case of Cadmium-Imidazolate Framework, there is no research in this context according to the best of authors' knowledge.

Inspired by the above, this paper aims to investigate, experimentally and theoretically, the potential of using Cd-ZIF-8 as an adsorbent for removing methyl orange (MO) from contaminated water. The preparation of ZIF-8 by cadmium instead of zinc is expected to alter its geometry and flexibility, and thus its mechanical stability, transport properties, and its sorption characteristics (Sapnik et al., 2018). Indeed, divalent cadmium metal, which has a larger ionic radius than zinc (0.78 vs. 0.60 Å) is best placed to influence mechanical properties (Ohkubo et al., 2002). Therefore, the Cd-ZIF-8 is expected

to have increased stability, which is very interesting from a practical engineering perspective (Sun et al., 2018; Xu et al., 2019). Furthermore, it is reported that ZIF-8 has the potential to remove MO from wastewater; however, its adsorption capacity (between 1.8 and 45.82 mg g⁻¹) is not sufficient for a successful MO removal process (Ding et al., 2017; Y. Li et al., 2016; Zhang et al., 2020). Thus, we assume that altering ZIF-8's properties by using Cd will have a positive effect on its adsorption ability. The prepared material was characterized by XRD, BET, FT-IR and SEM techniques. Then, its adsorption capability for the successful removal of methyl orange (MO) was studied in detail. Besides, to clarify whether there will be a potential release of cadmium ions into the treated wastewater, the stability of the prepared material was evaluated at different pH and its structure after adsorption was checked by XRD. Besides, Density Functional Theory (DFT) cluster calculations were employed to shed light on the interactions between Cd-ZIF-8 and the methyl orange (MO) molecule.

2. Materials and methods

2.1. Chemicals

The following chemicals: Cadmium nitrate hydrate (Cd(NO₃)₂·6H₂O, 99.5%, Sigma-Aldrich) as a source for metal ions, 2-methylimidazole (C₄H₅N₂, 97%, Sigma-Aldrich) as a source for the linker, methanol (99.8%, Sigma-Aldrich) as a solvent, and methyl orange (MO) as a model pollutant were employed in the present work. All materials were used as purchased without any further purification.

2.2. Synthesis of Cd-ZIF-8

In a typical synthesis, the metal solution was obtained by dissolving 1.47 g of cadmium nitrate hydrate in 100 mL of methanol with stirring. In a separate portion of methanol, the ligand solution was prepared by 3.25 g of 2-methylimidazole (2-mIm) in the same quantity of methanol. The mixed solution was collected by centrifugation at 7500 rpm for 30 min, redispersed in ethanol for removing unreacted linkers, and collected again by centrifugation. The resulting Cd-ZIF-8 was placed into an autoclave and heated at 60 °C for 48 h. Prior to characterization, the powder was collected, washed with fresh methanol, and dried under vacuum at room temperature.

2.3. Characterization techniques

Nitrogen adsorption-desorption isotherms were carried out for textural characterization of Cd-ZIF-8 using a Micromeritics ASAP 2020 adsorption analyzer (USA) at liquid nitrogen temperature (77 K). The Brunauer-Emmett-Teller (BET-60H, Shimadzu, Japan) was employed to determine the surface areas, pore size distribution, and pore volume. The powder X-ray diffraction (XRD) of Cd-ZIF-8 was measured from 2θ = 5° to 50° using an X-ray diffractometer (XRD, X'pert MPD PRO, Philips) using Cu-Kα (λ = 1.54 Å) radiation. Infrared (IR) spectra were recorded in the range of 400–4000 cm⁻¹ with a resolution of 4 cm⁻¹ using Shimadzu FTIR Spectrophotometer (Shimadzu JASCO 4100, Tokyo, Japan). The morphology of Cd-ZIF-8 was investigated using Scanning Electron Micro-

scope (SEM, Topcon model EM200B) with 200 kV acceleration voltage.

2.4. Adsorption experiments

Batch type experiments were carried out at a temperature range from 30 to 50 °C. Different initial concentrations of MO (50, 100, 150, and 200 mg/L) were used to study the effect of contact time. This was done by mixing a 1.7 g of Cd-ZIF-8 with V = 10 mL of MO solution using a stirring rate of 600 rpm and a solution pH = 2. The effect of adsorbent mass was evaluated by adding different masses of Cd-ZIF-8 (0.5 to 3.5 g) to V = 10 mL of MO solution with initial concentration C₀ = 200 mg/L. The pH of the solution was controlled by adding HCl (0.1 M) and NaOH (0.1 M). At pre-set times, the remaining MO solution was analyzed and its residual concentration at equilibration time *t* (min), (C_e, in mg/L) was determined by a UV-vis photospectrometer (Shimadzu, UV-1240) at 460 nm. C₀ and C_e values were used to estimate the amount of MO adsorbed on the Cd-ZIF-8, at each equilibrium, q_e (mg/g) employing the following equation (Dehmani et al., 2020).

$$q_e = \frac{C_0 - C_e}{m_{ads}} \times V_{sol} \quad (1)$$

where *m*_{ads} is the Cd-ZIF-8 mass (in g) and *V*_{sol} is the volume of the solution (L).

Different equilibrium isotherm and adsorption kinetic models were used to study the adsorption process. The nonlinear curve fitting method by Origin software (OriginLab, V8.5) was employed to fit kinetic and isotherm models to the experimental data. Equations of all used isotherm and kinetic models were described in Table S1 (Supplementary Material). To guarantee the reliability of results, each experiment was triplicate and averaged.

2.5. Desorption and stability experiments

To explore the reusability of the prepared Cd-ZIF-8 after adsorption, the adsorbent was de-adsorbed through repeated washing with ethanol and then dried before performing adsorption-desorption cycles. Five cycles were done, and the removal efficiency was determined by UV-vis spectrum. On the other hand, the stability of the prepared Cd-ZIF-8 after the adsorption was evaluated by XRD and the potential release of cadmium ions was studied at different pH values.

2.6. Theoretical studies

DFT cluster calculations were carried out to get insights into the adsorption mechanism of MO on Cd-ZIF-8. To this end, and to reduce the computational cost, four clusters were considered for DFT calculations. Employing cluster models is a common method for studying dye-ZIF-8 interactions and for other MOFs (Chizallet et al., 2010; Liu and Zhong, 2010; Ryan et al., 2012). Clusters used in our calculations were inspired by the work of Chizallet et al. (Chizallet et al., 2010), where readers can find a detailed description of each cluster. Geometry optimizations, highest occupied (HOMO), and lowest (LUMO) unoccupied molecular orbitals were all determined by using B3LYP exchange-correlation function with 6-31G(d, p) basis set for C, N, and H atoms and the

LANL2DZ basis set for Cd. GaussView 5.0.8 and Gaussian 09 programs were used to generate/visualize structure and DFT calculations, respectively (Frisch, 2009).

3. Results and discussion

3.1. Characterization of Cd-ZIF-8

XRD patterns were performed to analyze the phase structure and purity of prepared Cd-ZIF-8. Phase analysis and unit cell parameters were determined using Fullprof software (Rodríguez-Carvajal, 2001) based on the Rietveld method, as shown in Fig. 1(a). XRD reveals that as-prepared Cd-ZIF-8 possesses a cubic-phase structure with an $I43m$ space group, in good agreement with earlier reports (Fairen-Jimenez et al., 2011). Results also show that Cd-ZIF-8 exhibits a lattice constant of 16.992 Å and a unit cell volume of 4833.41 Å³. The analysis of XRD patterns (excluding those with very low yield and impure product) show 2θ diffraction peaks at $2\theta = 7.3^\circ, 10.25^\circ, 12.74^\circ, 14.76^\circ, 16.33^\circ, 18.1^\circ, 19.43^\circ, 21.87^\circ, 25.6^\circ, 26.41^\circ,$ and 28.41° representing the (0 1 1), (0 0 2), (1 1 2), (0 2 2), (0 1 3), (2 2 2), (1 2 3), (1 1 4), (2 2 4), (1 3 4), and (0 4 4) plane reflections (Akbari Beni et al., 2020; Fairen-Jimenez et al., 2011; Park et al., 2006). Results demonstrate that experimental XRD patterns match well with the simulated one, indicating the powder samples are phase-pure Cd-ZIF-8. The structure of Cd-ZIF-8, which is a sodalite (SOD) zeolite-type structure exhibit four-coordinated cadmium N atoms of 2-

mIm ligand in a tetrahedral geometry. The crystallize size D was calculated using the Scherrer equation:

$$D = 0.9\lambda / \beta \cos\theta \quad (2)$$

where, λ is the wavelength of X-ray (1.54 Å), β corresponds to the full width at half maxima (FWHM), θ is the diffraction angle. The estimated size of Cd-ZIF-8 sample is about 300 nm.

The analysis of the FT-IR spectrum is shown in Fig. 1(b). The FT-IR spectrum shows peaks at 600–1600 cm⁻¹ attributed to the entire ring stretching or bending modes. The absorption peaks at 2912 cm⁻¹, corresponding to the aromatic C–H stretch of the imidazole. Interestingly, the absorption peak at 450 cm⁻¹ is attributed to the Cd–N stretching. Tsai et al. (Tsai et al., 2019) confirmed that the absence of a broad peak between 3000 and 3500 cm⁻¹ is an indication of the substitution of the imidazole ligand and the cadmium on the N–H bond, suggesting successful bonding of metal Cd and 2-methylimidazole ligands.

Morphology of the prepared Cd-ZIF-8 was examined by SEM and represented in Fig. 1(c). The SEM image shows that Cd-ZIF-8 possesses micrometer-sized crystals with uniform cubic shapes, which conforms with the typical form of ZIF-8 (Abdi et al., 2017; He et al., 2014; Wang et al., 2020).

Specific surface areas and porosity of the as-prepared Cd-ZIF-8 were determined by N₂ adsorption-desorption isotherm at 77 K. The pore size was calculated by Barrett–Joyner–Halenda (BJH) analysis. The isotherm is shown in Fig. 1(d) while BET morphological parameters are listed in Table 1. The Cd-ZIF-8 has primarily micropores; however, the increase of the

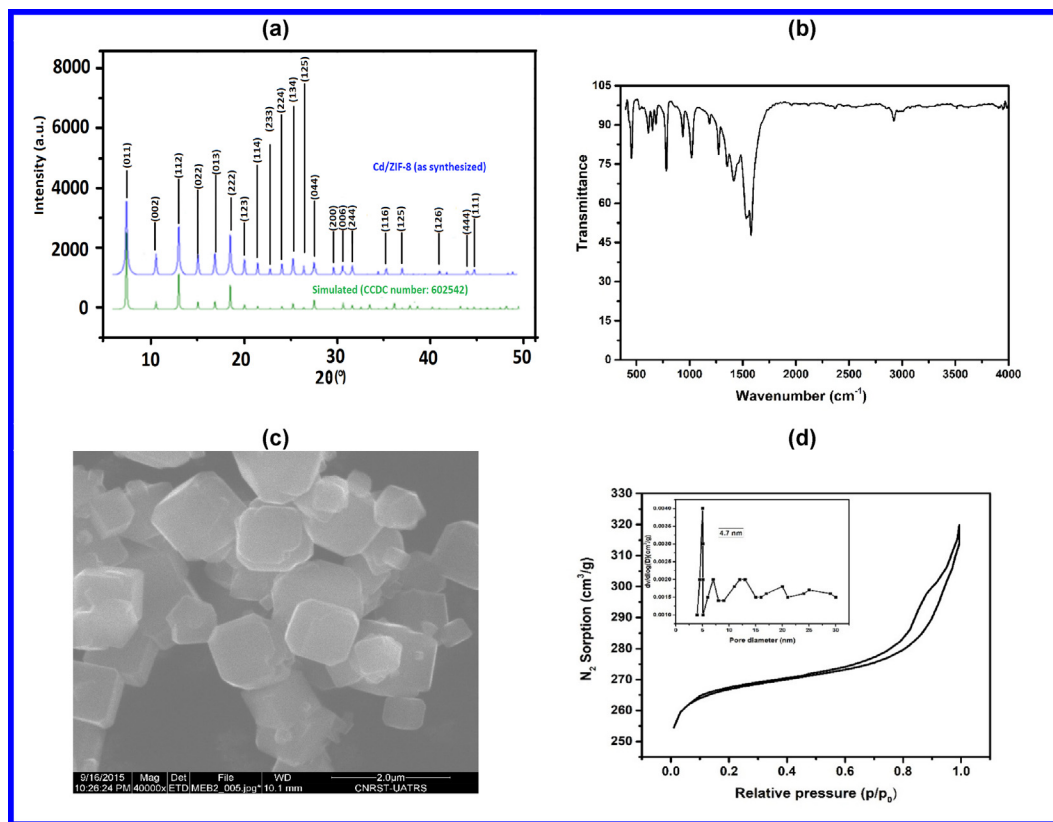


Fig. 1 (a) Powder X-ray diffraction patterns, (b) FT-IR, (c) SEM micrograph and (d) N₂ adsorption-desorption isotherm (inset pore size distribution plot) of Cd-ZIF-8.

Table 1 Surface areas, pore size and pore volume parameters of Cd-ZIF-8.

Sample	BET Surface area ($\text{m}^2 \text{g}^{-1}$)	Langmuir Surface area ($\text{m}^2 \text{g}^{-1}$)	Average pore diameter (\AA)	Total pore Volume (g^{-1})	<i>t</i> -method micro pore volume (g^{-1})	Pore size distribution (nm)
Cd/ZIF-8	1281	1776	12	0.62	0.61	4.7

type IV isotherm in the higher pressure region $P/P_0 = 0.7\text{--}1.0$ suggests the presence of mesopores, which might be attributed to the packing of particles with smaller size or the existence of structural defects in the framework where higher interaction energy with water molecules occurs (Guan et al., 2017; Zhang et al., 2020). These defects are expected to play a vital role in improving the adsorption efficiency. Besides, textural characteristics of Cd-ZIF-8 tabulated in Table 1 show BET and Langmuir surface areas of 1281 and 1776 m^2/g , respectively. Further, the average pore diameter equals 12 \AA , and the pore size distribution is 4.7 nm.

3.2. MO adsorption onto the Cd-ZIF-8

3.2.1. Effect of initial MO concentration and contact time

A key factor in determining the efficiency of an adsorption process is knowing the suitable time of contact between an adsorbate and the adsorbent that allows maximum adsorption. Fig. 2 illustrates the influence of contact time on the amount of MO adsorbed onto the Cd-ZIF-8 samples at 50, 100, 150, and 200 mg/L of MO. Experiments were undertaken in the 0–480 min time interval. As expected, a higher adsorption rate is obtained at higher MO concentration. In the initial 50 min of adsorption, results in Fig. 2 show a sharp increase in the MO adsorption rate, and equilibrium was attained in about 60 min. After this time, the MO adsorption rate remains constant despite prolonged contact time. The Cd-ZIF-8 showed a rapid rate for methyl orange for the first 60 min, owing to the presence of vacant sites in Cd-ZIF-8. In such a situation, the positively charged Cd^{2+} in Cd-ZIF-8 and the sulfonate group of the MO can form ionic bonding, thus facilitating MO adsorption (Jung et al., 2015). As time increases, the available sites for adsorption become fewer and saturation is reached.

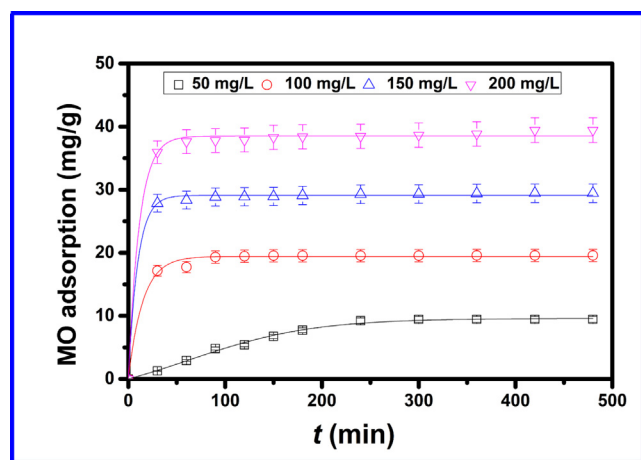


Fig. 2 The effect of the contact time on the adsorption of MO at different concentrations onto Cd-ZIF-8.

The adsorption at this stage becomes more difficult because of electrostatic repulsions between free and adsorbed MO molecules (Maneerung et al., 2016).

3.2.2. Effect of pH and adsorbent dosage

In the adsorption process, pH is an essential factor; it can impact adsorbate states and the surface charges of adsorbents. Therefore, the effect of pH on the removal of MO by Cd-ZIF-8 is evaluated, and results are represented in Fig. 3. Experiments were performed in a wide range of pH. We observe from the obtained results that alkaline conditions are less favorable for adsorption of MO with only 40% at $\text{pH} = 10$. At lower pH, the adsorption capacity of MO dye is higher at pH between 2 (92 mg/g) and 3 (90 mg/g), and then it started decreasing. This reflects that pH is an essential factor affecting MO adsorption onto Cd-ZIF-8.

The optimization of the adsorbent amount is another significant parameter in determining optimum conditions for adsorption. The influence of Cd-ZIF-8 amount on the percentage removal of MO is shown in Fig. S1 (supplementary material). The obtained results reveal that, with increasing adsorbent dose from 0.5 to 1.7 g, the MO adsorption increases sharply, and removal percentages increase from 40% to 100%. At this point, MO removal reaches saturation, and no more variations are seen. As the amount of Cd-ZIF-8 increases, the number of available binding sites for the adsorption increases, which in turn yields to higher MO adsorption. A constant removal yield is observed despite further increases in the adsorbent amount.

3.2.3. Adsorption kinetics

In the adsorption process, the challenge is to figure out the adsorption mechanism and what parameters are critical in con-

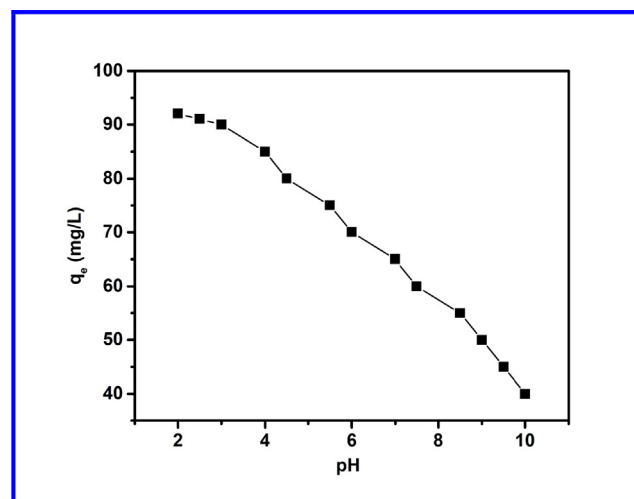


Fig. 3 Effect of pH on the removal of MO by Cd-ZIF-8.

trolling the effectiveness of an adsorbent. To approach this aim, experimental data at different initial dye concentrations corresponding to various contact times were fitted to the most widely used kinetic models, i.e., the pseudo-first-order (PFO) and pseudo-second-order (PSO) models, as shown in Fig. 4. Kinetic parameters and correlation coefficients are listed in Table 2. The Lagergren kinetic rate equation has been widely used for the explication of adsorption kinetics of organic molecules in aqueous solutions. Those include studies on dyes adsorption by MOFs, which have shown the suitability of PFO model (Jing et al., 2014; Mohd Tahir et al., 2017). Based on correlation coefficients and adsorption capacities at different MO concentrations (Table 2), it appears that kinetics data from PFO model does not match well with experimental results. Hence, suggesting that the PFO model does not control the MO adsorption by Cd-ZIF-8, which is in consistent with results from many adsorption systems (Kumar, 2006; Wong et al., 2004). Results in Table 2 also show PSO's kinetics data. The applicability of the PSO model in describing the adsorption of organic molecules on ZIF-8 has already been demonstrated (Feng et al., 2016; Jiang et al., 2013). Data in Table 2 show higher correlation coefficients and adsorption capacities close to experimental ones at all MO concentrations, indicat-

ing the methyl orange adsorption on Cd-ZIF-8 correlates very well with the PSO kinetic model. The pseudo-second order model assumes that the rate of the adsorption is a function of the number of sites available for adsorption and the dye concentration.

Interestingly, the rate constant for the PSO model decreases with the increase of the MO initial concentration, suggesting that chemisorption is implicated in the rate-limiting step (Jiang et al., 2013). In this case, the exchange of electrons between the adsorbent and the adsorbate takes place via exchange or sharing of electrons, i.e., complexation or coordination process. The pseudo-second order model takes these valency forces into account which makes it better than the pseudo-first-order model in describing the adsorption process in this work (Huo and Yan, 2012; Qi et al., 2013).

3.2.4. Adsorption isotherms and thermodynamic parameters

The determination of the adsorption isotherm is a powerful way to understand MO adsorption processes over Cd-ZIF-8. It helps in getting insights about the interaction between adsorbate and adsorbent at the equilibrium state (Chen et al., 2019). To achieve this aim, Langmuir and Freundlich isotherms,

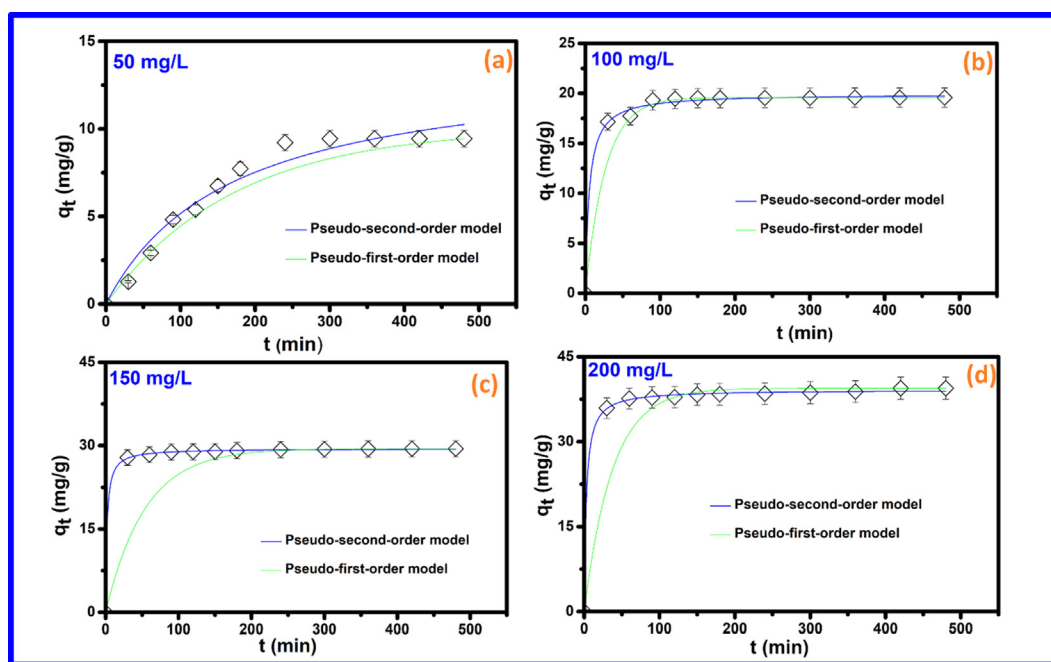


Fig. 4 Pseudo-first order and Pseudo-second order kinetic plots obtained for various concentrations of MO. (a) 50 mg/L, (b) 100 mg/L, (c) 150 mg/L, and (d) 200 mg/L.

Table 2 Kinetic analysis of MO adsorption on Cd-ZIF-8.

[MO] (mg/L)	$q_{e, \text{exp}}$ (mg/g)	Pseudo-first-order kinetic model			Pseudo-second-order kinetic model		
		$q_{e, \text{cal}}$ (mg/g)	k_1 (h^{-1})	R^2	$q_{e, \text{cal}}$ (mg/g)	k_2 (g/mg min)	R^2
50	9.43	6.89	2.124	0.89	9.83	0.049	0.98
100	19.57	14.14	0.004	0.94	19.96	0.042	0.99
150	29.43	28.98	6.140	0.95	29.46	0.017	0.99
200	39.43	38.24	0.009	0.95	39.16	0.008	0.99

which are well-known isotherm models, were applied to fit the MO adsorption data at different temperatures. Isotherm plots in Fig. 5 show that, when the temperature increases, the adsorption capacity for methyl orange is simultaneously enhanced. This behavior generally is explained by the increase in the chemical affinity of the adsorbate (MO) to the Cd-ZIF-8 surface, during which chemical interactions are assumed to take place (Dehmani et al., 2020). Table 3 lists the values of the coefficient of determination and isothermal parameters derived from Langmuir and Freundlich isotherm plots. Results reveal that the Langmuir model is more applicable than the Freundlich model in modeling the MO adsorption over Cd-ZIF-8. Maximum adsorption capacities of Cd-ZIF-8 derived from Langmuir isotherm model are 93.24, 101.32 and 145.41 mg/g at 30°, 40°, and 50° temperatures, respectively. The Langmuir isotherm model implies that each adsorbate molecule is adsorbed homogeneously at a fixed number of localized sites on the adsorbent's surface and negligible interactions between adsorbed molecules (Mathurasa and Damrongsiri, 2018; Omotunde et al., 2018). Based on this, it is plausible to assume that the adsorption is mainly monolayer and that the adsorbent (Cd-ZIF-8) has uniform adsorption energy.

Furthermore, thermodynamic parameters were computed for a more detailed examination of the interaction between MO molecules and Cd-ZIF-8 surface. To this end, and for a precise measurement of thermodynamic adsorption parameters, dimensionless thermodynamic equilibrium constants are calculated at different temperatures, by using the equation below (Lima et al., 2019):

$$K_e^\circ = \frac{(1000 \times K_L \times \text{molecular weight of adsorbate}) \times [\text{Adsorbate}]^\circ}{\gamma} \quad (3)$$

In this equation, γ denotes the adsorbate's coefficient of activity (dimensionless, taken as unity) (Atkins and De Paula, 2011), $[\text{Adsorbate}]^\circ$ refers to the standard concentration of MO (1 mol L⁻¹) (Chang and Thoman, 2014), and K_L is the isotherm constant. Then, dimensionless thermodynamic equilibrium constants were used to estimate entropy change (ΔS°), enthalpy change (ΔH°), and free energy change (ΔG°) of adsorption based on the following equations (Lima et al., 2019):

$$\Delta G^\circ = -RT \ln(K_e^\circ) \quad (4)$$

$$\ln(K_e^\circ) = \frac{-\Delta H^\circ}{R} \times \frac{1}{T} + \frac{\Delta S^\circ}{R} \quad (5)$$

In these equations, T and R denote the temperature (in K) and the universal gas constant (8.314 J K⁻¹ mol⁻¹), respectively.

In Fig. S2, a linear relationship is observed between $\ln(K_e^\circ)$ and $1/T$, and therefore enthalpy and entropy changes were calculated and listed in Table 3 along with Gibbs free energy change values. Results in Table 3 show negative ΔG° values at all temperatures, which reflect the spontaneous and feasibility of the MO adsorption onto the Cd-ZIF-8 surface (Rahman and Sathasivam, 2015). Additionally, results show positive signs of enthalpy and entropy changes, suggesting an endothermic and random adsorption process at Cd-ZIF-8/solution interphase, respectively (S. Liu et al., 2020).

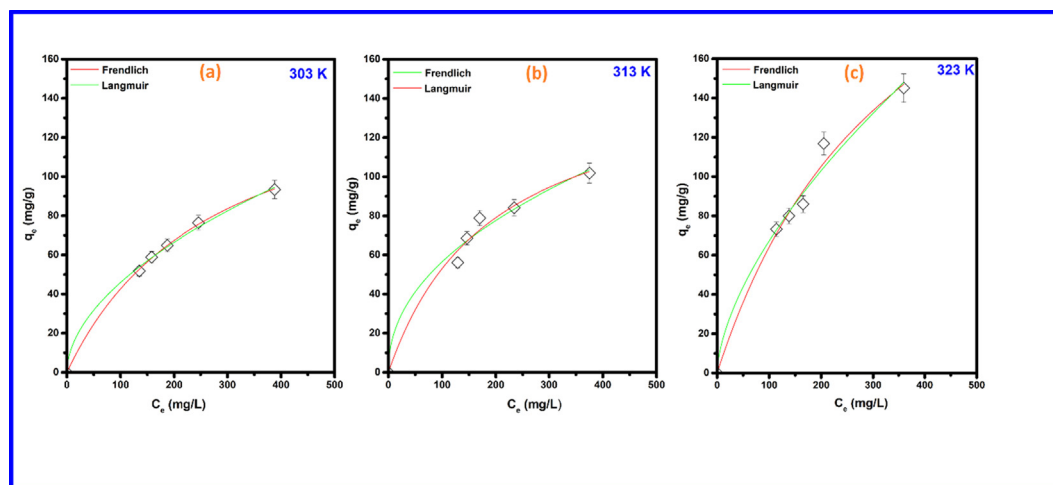


Fig. 5 Adsorption isotherms for MO on Cd-ZIF-8 at different temperatures. (a) 303 K, (b) 313 K, and (c) 323 K.

Table 3 Isotherm parameters for MO adsorption on Cd-ZIF-8.

Temperature(°)	Langmuir Isotherm						Freundlich Isotherm		
	q_m (mg/g)	K_L (L/mg)	R^2	ΔG° (kJ/mol)	ΔH° (kJ/mol)	ΔS° (kJ/mol)	K_F (mg/g)	$1/n$	R^2
30	93.24	0.003	0.996	-17.35			3.95	0.605	0.965
40	101.32	0.005	0.987	-19.25	34.52	171.43	4.17	0.532	0.966
50	145.41	0.002	0.987	-20.77			6.86	0.450	0.973

3.3. Reusability test and comparison with other adsorbents

To make the adsorption process cost-effective, a promising adsorbent should have a high recycling ability, which could open the way to pilot-scale applications. Herein, we also investigated whether prepared Cd-ZIF-8 could regenerate its adsorption sites by performing five adsorption/desorption cycles. Regeneration cycles are displayed in Fig. 6, where we can see MO removal percentage dropping slightly after five runs of adsorption/desorption process. After the first cycle, which shows the highest value (95%), a slight decrease in MO regeneration can be observed. It reaches 87% at the fifth cycle, which can be due to a decrease in available sites for adsorption. The higher removal percentage after five cycles is an indication for the excellent applicability of the prepared Cd-ZIF-8 for repetitive use in dyes removal.

On the other hand, Table 4 lists adsorption capacity for the removal of methyl orange by some adsorbents, as reported in the literature. The reported data show that the maximum MO uptake of Cd-ZIF-8 is comparatively higher than that of ZIF-8 and some other adsorbents, suggesting its good practical applications in dyes treatment and the usefulness of using cadmium-based ZIF-8 for removal of MO. However, further functionalization would have a significant influence on its application in dyes removal.

3.4. The stability test of the prepared Cd-ZIF-8

While the use of the cadmium instead of the zinc in ZIF-8 is beneficial in terms of adsorption capacity, the potential release of cadmium ions into the treated water should be considered for safe application in water treatment. Like other heavy metals, which are toxic or poisonous at low concentrations, cadmium (Cd) is a cumulative toxin with a long biological half-life (> 30 years) and harmful effects on the ecosystem (Gautam et al., 2014). Therefore, in this work, the stability of the prepared Cd-ZIF-8 at different pH values was evaluated. The amount of Cd^{2+} released from Cd-ZIF-8 was quantitatively detected by Spectrometer ICP-OES after being placed in water for 7 days in different pH solutions at room

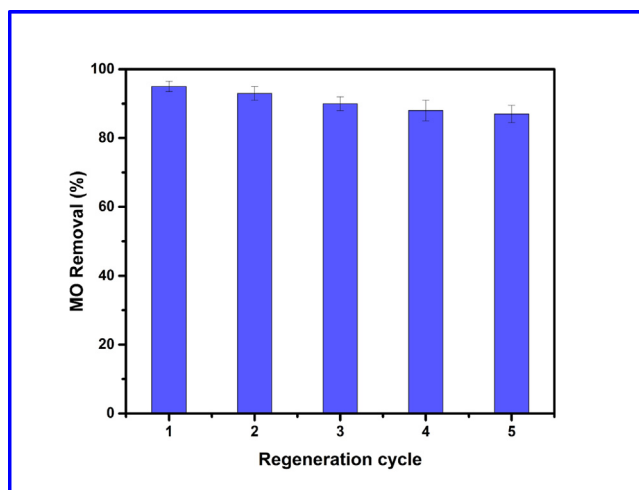


Fig. 6 Recycling performance of Cd-ZIF-8 in the removal of MO.

Table 4 Comparison of adsorption capacity of various adsorbents at 298 K with that of Cd-ZIF-8 for removal of MO.

Adsorbent	Adsorption capacity (mg g^{-1})	Reference
Carboxymethyl cellulose	39.47	Yu et al. (2018)
Graphene oxide	16.83	Robati et al. (2016)
$\text{Ni}_{0.05}\text{Zn}_{0.95}\text{O}$	23	Klett et al. (2014)
Hexagonal shaped nanoporous Carbon	18.08	Kundu et al. (2017)
MIL-53 (Cr)	57.9	Haque et al. (2010)
PED-MIL-101	194.0	Haque et al. (2010)
MOF-235	477	Haque et al. (2011)
MIL-100 (Cr)	211.8	Mehmandoust et al. (2019)
MIL-100 (Fe)	1045.2	Mehmandoust et al. (2019)
pillar[5]arene-modified zeolite	8.33	Yang et al. (2019)
cross-linked chitosan	89.29	Huang et al. (2017)
ZIF-8 ($1008 \text{ m}^2 \text{ g}^{-1}$)	1.8	Y. Li et al. (2016)
ZIF-8 ($1291 \text{ m}^2 \text{ g}^{-1}$)	45.82	Ding et al. (2017)
ZIF-8 ($1426 \text{ m}^2 \text{ g}^{-1}$)	5.22	Zhang et al. (2020)
Cd-ZIF-8	93.24	Present work

temperature and results are represented in Fig. 7(a). Besides, the X-ray diffraction patterns (Fig. 7(b)) of the Cd-ZIF-8 were determined to examine the phase arrangement and crystalline nature of the prepared material after the adsorption tests. Given the excellent adsorption effect of this adsorbent on MO in high pH solutions, we investigated its stability in the pH range of 2–12. As shown in Fig. 7(a), the amount of Cd^{2+} released from Cd-ZIF-8 is practically zero in the pH range 2–10, while it does not exceed 0.3% at pH = 12. These results indicate that the adsorbent maintains sufficient stability in a wide pH range. Furthermore, after the adsorption of MO dye molecules on Cd-ZIF-8, there are no changes observed in the diffraction patterns which emphasize the chemical stability of the prepared material and its safe use in removal of MO dye (Sirajudheen et al., 2020).

3.5. DFT computational studies of possible adsorption mechanisms

Understanding the adsorption mechanisms of an adsorbate molecule on the surface of an adsorbent is of paramount importance to explain interactions between them and for the optimal design of future adsorbents in this class (Dong et al., 2019). In the present section, attempts were made to search for possible adsorption mechanisms that govern the interactions between MO molecules and Cd-ZIF-8 surface by employing cluster DFT calculations. The idea of using the cluster approach to investigate adsorbate-ZIF-8 interactions was proved to be powerful in previous works, in which researchers confirmed its accuracy compared to using the periodic structure (Chizallet et al., 2010; Chizallet and Bats, 2010). Investiga-

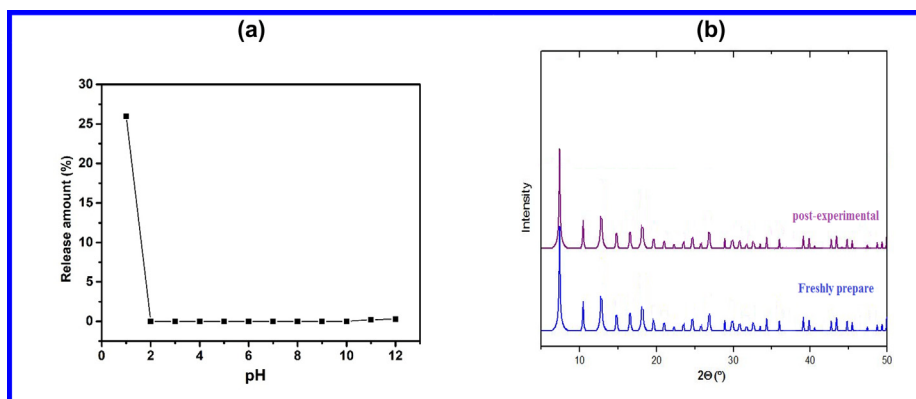


Fig. 7 (a) XRD patterns of Cd-ZIF-8 after adsorption, and (b) release of Cd ions at different pH values.

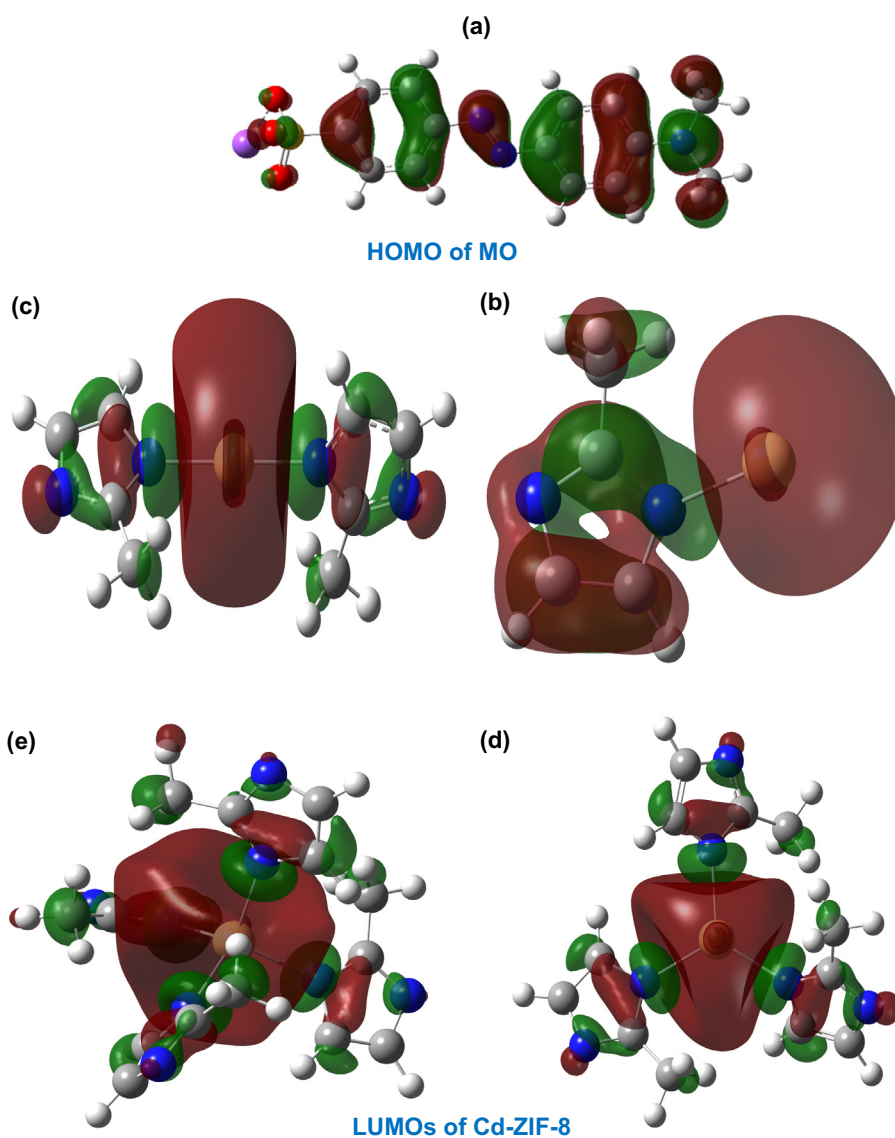


Fig. 8 DFT computationally predicted HOMO of the methyl orange (a) and LUMOs of Cd-ZIF-8 (b-e). Cd-ZIF-8 is represented by a cluster of $\{Cd(2-mIm)_x\}^{2-x}$ with x is an integer from 4 (model (b)) to 1 (model (e)).

tion of electronic properties of MO and Cd-ZIF-8 through frontier molecular orbitals, i.e., the highest occupied molecular orbital (HOMO) and the lowest unoccupied molecular orbitals (LUMO) could be of tremendous help in identifying potential interactions. The HOMO density distribution of methyl orange and LUMO density distribution of Cd-ZIF-8 (including partially de-coordinated Cd sites) is shown in Fig. 8. In this Figure, clusters with 1 ($\{Cd(2-mIm)\}^+$), 2 ($\{Cd(2-mIm)_2\}^0$), and 3 ($\{Cd(2-mIm)_3\}^-$) ligands represent structures with open metal defects. In contrast, that with 4 ($\{Cd(2-mIm)_4\}^{2-}$) ligands represents the tetrahedrally coordinated Cd. Fig. 8 shows that the HOMO density of MO is distributed over the entire molecular structure, whereas the isodensity in LUMO of defective Cd-ZIF-8 clusters is largely dispersed on the low coordinated Cd ion. In this case, Cd ions will exhibit Lewis acid properties, and therefore it is possible to predict that open Cd sites will interact with different parts of MO molecules, forming a Lewis acid/base complex (Liu et al., 2015). This kind of electrostatic interactions is expected to be more pronounced when considering clusters with fewer 2-mIm ligands, and this can be well observed from the larger LUMO distribution over $\{Cd(2-mIm)\}^+$, $\{Cd(2-mIm)_2\}^0$, and $\{Cd(2-mIm)_3\}^-$ clusters. In this manner, MO molecules can be easily attracted to the open Cd sites due to the little steric hindrance effect. In contrast, such behavior would be less significant in the case of tetrahedrally coordinated Cd-ZIF-8 ($\{Cd(2-mIm)_4\}^{2-}$ cluster) due to the strong steric hindrance effect that will make interactions between MO molecules and Cd-ZIF-8 difficult. Furthermore, the imidazole ring in 2-mIm could play a key role in interactions between adsorbate's molecules and the adsorbent. Its electron-rich nitrogen atoms and double bonds may potentially interact with the aromatic rings of MO via the π - π stacking interaction, while hydrogen atoms may be involved in hydrogen bonding (Hasan and Jung, 2015). All of these interactions, which were previously reported in the case of the adsorption of organic pollutants to MOFs (Abdi et al., 2017; Hasan and Jung, 2015; Mahmoodi, 2014), provide rich insights into how MO molecules can interact with Cd-ZIF-8.

4. Conclusion

The present study explored the successful use of a synthesized cadmium zeolitic-imidazolate framework (Cd-ZIF-8) for adsorption and removal of methyl orange from aqueous solution at different operating conditions. The prepared material was characterized and confirmed by XRD, BET, FT-IR, and SEM techniques. The BET analysis showed a micro/mesoporous structure, with account for 98.38% of the total pore volume, while SEM analysis showed micrometer-sized crystals with uniform cubic shapes. The Langmuir isotherm was found to fit more satisfactory than the Freundlich isotherm the favorable adsorption of MO onto the adsorbent. The corresponding maximum adsorption capacity was equal to 93.24 mg/g. The obtained thermodynamic parameters indicated an endothermic adsorption process, thus raising the temperature led to a greater MO adsorption. The kinetic study showed that MO adsorption on Cd-ZIF-8 followed a PSO model, suggesting that the prevailing adsorption mechanism is chemisorption. The adsorption-desorption efficiency of the Cd-ZIF-8 was examined up to five successive cycles and showed an excellent reusability performance. Furthermore, the prepared material

showed good stability after the adsorption tests with no release of Cd ions at a wide range of pH. Cluster DFT calculations provided insights into the adsorption mechanism and predicted electrostatic interactions, π - π stacking interactions, and hydrogen bonding as main interactions between MO molecule and Cd-ZIF-8. Based on the results of the present work, the proposed material could be considered as an excellent adsorbent for effective dye removal and thereby opens new paths for further research.

Declaration of Competing Interest

The authors declare that they have no known competing financial interests or personal relationships that could have appeared to influence the work reported in this paper.

Acknowledgement

This work was supported by the Institute of Research and Consulting Studies at Umm Al-Qura University (Grant Code. 19-SCI-1-01-0006).

Appendix A. Supplementary material

Supplementary data to this article can be found online at <https://doi.org/10.1016/j.arabjc.2020.11.003>.

References

- Abdelhamid, Hani Nasser, 2020a. Dye encapsulated hierarchical porous zeolitic imidazolate frameworks for carbon dioxide adsorption. *J. Environ. Chem. Eng.* 8, 104008. <https://doi.org/10.1016/j.jece.2020.104008>.
- Abdelhamid, H.N., 2020b. Zinc hydroxide nitrate nanosheets conversion into hierarchical zeolitic imidazolate frameworks nanocomposite and their application for CO₂ sorption. *Mater. Today Chem.* 15, 100222. <https://doi.org/10.1016/j.mtchem.2019.100222>.
- Abdelhamid, H.N., Huang, Z., El-Zohry, A.M., Zheng, H., Zou, X., 2017. A fast and scalable approach for synthesis of hierarchical porous zeolitic imidazolate frameworks and one-pot encapsulation of target molecules. *Inorg. Chem.* 56, 9139–9146. <https://doi.org/10.1021/acs.inorgchem.7b01191>.
- Abdel-Magied, A.F., Abdelhamid, H.N., Ashour, R.M., Zou, X., Forsberg, K., 2019. Hierarchical porous zeolitic imidazolate frameworks nanoparticles for efficient adsorption of rare-earth elements. *Microporous Mesoporous Mater.* 278, 175–184.
- Abdi, J., Vossoughi, M., Mahmoodi, N.M., Alemzadeh, I., 2017. Synthesis of metal-organic framework hybrid nanocomposites based on GO and CNT with high adsorption capacity for dye removal. *Chem. Eng. J.* 326, 1145–1158. <https://doi.org/10.1016/j.cej.2017.06.054>.
- Akbari Beni, F., Gholami, A., Ayati, A., Niknam Shahrak, M., Sillanpää, M., 2020. UV-switchable phosphotungstic acid sandwiched between ZIF-8 and Au nanoparticles to improve simultaneous adsorption and UV light photocatalysis toward tetracycline degradation. *Microporous Mesoporous Mater.* 303, 110275. <https://doi.org/10.1016/j.micromeso.2020.110275>.
- Alqaragully, M.B., 2014. Removal of textile dyes (maxilon blue, and methyl orange) by date stones activated carbon. *Int. J. Adv. Res. Chem. Sci.* 1, 48–59.
- Atkins, P., De Paula, J., 2011. *Physical Chemistry for the Life Sciences*. Oxford University Press, USA.
- Bulgariu, L., Escudero, L.B., Bello, O.S., Iqbal, M., Nisar, J., Adegoke, K.A., Alakhras, F., Kornaros, M., Anastopoulos, I.,

2019. The utilization of leaf-based adsorbents for dyes removal: a review. *J. Mol. Liq.* 276, 728–747. <https://doi.org/10.1016/j.molliq.2018.12.001>.
- Chang, R., Thoman, J.W., 2014. *Physical Chemistry for the Chemical Sciences*. University Science Books.
- Chen, X., Jiang, X., Yin, C., Zhang, B., Zhang, Q., 2019. Facile fabrication of hierarchical porous ZIF-8 for enhanced adsorption of antibiotics. *J. Hazard. Mater.* 367, 194–204. <https://doi.org/10.1016/j.jhazmat.2018.12.080>.
- Chin, M., Cisneros, C., Araiza, S.M., Vargas, K.M., Ishihara, K.M., Tian, F., 2018. Rhodamine B degradation by nanosized zeolitic imidazolate framework-8 (ZIF-8). *RSC Adv.* 8, 26987–26997.
- Chizallet, C., Bats, N., 2010. External surface of zeolite imidazolate frameworks viewed ab initio: multifunctionality at the organic–inorganic interface. *J. Phys. Chem. Lett.* 1, 349–353.
- Chizallet, C., Lazare, S., Bazer-Bachi, D., Bonnier, F., Lecocq, V., Soyer, E., Quoineaud, A.-A., Bats, N., 2010. Catalysis of transesterification by a nonfunctionalized metal–organic framework: acid–basicity at the external surface of ZIF-8 probed by FTIR and ab initio calculations. *J. Am. Chem. Soc.* 132, 12365–12377.
- Chueh, C.-C., Chen, C.-I., Su, Y.-A., Konnerth, H., Gu, Y.-J., Kung, C.-W., Wu, K., 2019. Harnessing MOF materials in photovoltaic devices: recent advances, challenges, and perspectives. *J. Mater. Chem. A* 7, 17079–17095. <https://doi.org/10.1039/C9TA03595H>.
- Darwish, A., Rashad, M., AL-Aoh, H.A., 2019. Methyl orange adsorption comparison on nanoparticles: isotherm, kinetics, and thermodynamic studies. *Dyes Pigments* 160, 563–571.
- Dehmani, Y., Alrashdi, A.A., Lgaz, H., Lamhasni, T., Abouarnadasse, S., Chung, I.-M., 2020. Removal of phenol from aqueous solution by adsorption onto hematite (α -Fe₂O₃): mechanism exploration from both experimental and theoretical studies. *Arab. J. Chem.* 13, 5474–5486. <https://doi.org/10.1016/j.arabjc.2020.03.026>.
- Ding, Y., Xu, Y., Ding, B., Li, Z., Xie, F., Zhang, F., Wang, H., Liu, J., Wang, X., 2017. Structure induced selective adsorption performance of ZIF-8 nanocrystals in water. *Colloids Surf. Physicochem. Eng. Asp.* 520, 661–667. <https://doi.org/10.1016/j.colsurfa.2017.02.012>.
- Dong, X., Chen, S., Chen, Y., Zhang, M., 2019. Trace benzene removal from vinyl acetate with ZIFs: a computational study. *Comput. Theor. Chem.* 1158, 41–46. <https://doi.org/10.1016/j.comptc.2019.04.017>.
- El-Gamal, S., Amin, M., Ahmed, M., 2015. Removal of methyl orange and bromophenol blue dyes from aqueous solution using Sorel's cement nanoparticles. *J. Environ. Chem. Eng.* 3, 1702–1712.
- Fairen-Jimenez, D., Moggach, S., Wharmby, M., Wright, P., Parsons, S., Duren, T., 2011. Opening the gate: framework flexibility in ZIF-8 explored by experiments and simulations. *J. Am. Chem. Soc.* 133, 8900–8902.
- Farrusseng, D., Aguado, S., Pinel, C., 2009. Metal–organic frameworks: opportunities for catalysis. *Angew. Chem. Int. Ed.* 48, 7502–7513.
- Feng, Y., Li, Y., Xu, M., Liu, S., Yao, J., 2016. Fast adsorption of methyl blue on zeolitic imidazolate framework-8 and its adsorption mechanism. *RSC Adv.* 6, 109608–109612.
- Férey, G., 2008. Hybrid porous solids: past, present, future. *Chem. Soc. Rev.* 37, 191–214.
- Förstner, U., 2012. *Integrated Pollution Control*. Springer Science & Business Media.
- Frisch, A., 2009. gaussian 09W Reference. Wallingford USA, 25p.
- Gao, J., Qian, X., Lin, R.-B., Krishna, R., Wu, H., Zhou, W., Chen, B., 2020. Mixed metal–organic framework with multiple binding sites for efficient C₂H₂/CO₂ separation. *Angew. Chem. Int. Ed.* 59, 4396–4400. <https://doi.org/10.1002/anie.202000323>.
- Gautam, R.K., Sharma, S.K., Mahiya, S., Chattopadhyaya, M.C., 2014. CHAPTER 1 Contamination of Heavy Metals in Aquatic Media: Transport, Toxicity and Technologies for Remediation, pp. 1–24. <https://doi.org/10.1039/9781782620174-00001>.
- Guan, Y., Shi, J., Xia, M., Zhang, J., Pang, Z., Marchetti, A., Wang, X., Cai, J., Kong, X., 2017. Monodispersed ZIF-8 particles with enhanced performance for CO₂ adsorption and heterogeneous catalysis. *Appl. Surf. Sci.* 423, 349–353. <https://doi.org/10.1016/j.apsusc.2017.06.183>.
- Gupta, K., Khatri, O.P., 2019. Fast and efficient adsorptive removal of organic dyes and active pharmaceutical ingredient by microporous carbon: Effect of molecular size and charge. *Chem. Eng. J.* 378, 122218.
- Gupta, V.K., Suhas, 2009. Application of low-cost adsorbents for dye removal – a review. *J. Environ. Manage.* 90, 2313–2342. <https://doi.org/10.1016/j.jenvman.2008.11.017>.
- Haque, E., Jun, J.W., Jhung, S.H., 2011. Adsorptive removal of methyl orange and methylene blue from aqueous solution with a metal–organic framework material, iron terephthalate (MOF-235). *J. Hazard. Mater.* 185, 507–511.
- Haque, E., Lee, J.E., Jang, I.T., Hwang, Y.K., Chang, J.-S., Jegal, J., Jhung, S.H., 2010. Adsorptive removal of methyl orange from aqueous solution with metal–organic frameworks, porous chromium-benzenedicarboxylates. *J. Hazard. Mater.* 181, 535–542. <https://doi.org/10.1016/j.jhazmat.2010.05.047>.
- Hasan, Z., Jhung, S.H., 2015. Removal of hazardous organics from water using metal–organic frameworks (MOFs): Plausible mechanisms for selective adsorptions. *J. Hazard. Mater.* 283, 329–339. <https://doi.org/10.1016/j.jhazmat.2014.09.046>.
- He, M., Yao, J., Liu, Q., Wang, K., Chen, F., Wang, H., 2014. Facile synthesis of zeolitic imidazolate framework-8 from a concentrated aqueous solution. *Microporous Mesoporous Mater.* 184, 55–60. <https://doi.org/10.1016/j.micromeso.2013.10.003>.
- Hou, Y., Yan, S., Huang, G., Yang, Q., Huang, S., Cai, J., 2020. Fabrication of N-doped carbons from waste bamboo shoot shell with high removal efficiency of organic dyes from water. *Bioresour. Technol.* 303, 122939.
- Huang, R., Liu, Q., Huo, J., Yang, B., 2017. Adsorption of methyl orange onto protonated cross-linked chitosan. *Arab. J. Chem.* 10, 24–32. <https://doi.org/10.1016/j.arabjc.2013.05.017>.
- Huang, Y., Zeng, X., Guo, L., Lan, J., Zhang, L., Cao, D., 2018. Heavy metal ion removal of wastewater by zeolite-imidazolate frameworks. *Sep. Purif. Technol.* 194, 462–469.
- Huo, S.-H., Yan, X.-P., 2012. Metal–organic framework MIL-100 (Fe) for the adsorption of malachite green from aqueous solution. *J. Mater. Chem.* 22, 7449–7455.
- Jadhav, S.A., Garud, H.B., Patil, A.H., Patil, G.D., Patil, C.R., Dongale, T.D., Patil, P.S., 2019. Recent advancements in silica nanoparticles based technologies for removal of dyes from water. *Colloid Interface Sci. Commun.* 30, 100181.
- Jampa, S.S.K., Unnarkat, A.P., Vanshpati, R., Pandian, S., Sinha, M. K., Dharaskar, S., 2020. Adsorption and recyclability aspects of humic acid using nano-ZIF-8 adsorbent. *Environ. Technol. Innov.* 19, 100927. <https://doi.org/10.1016/j.eti.2020.100927>.
- Jiang, J.-Q., Yang, C.-X., Yan, X.-P., 2013. Zeolitic imidazolate framework-8 for fast adsorption and removal of benzotriazoles from aqueous solution. *ACS Appl. Mater. Interfaces* 5, 9837–9842.
- Jing, H.-P., Wang, C.-C., Zhang, Y.-W., Wang, P., Li, R., 2014. Photocatalytic degradation of methylene blue in ZIF-8. *RSC Adv.* 4, 54454–54462.
- Jung, B.K., Jun, J.W., Hasan, Z., Jhung, S.H., 2015. Adsorptive removal of p-arsanilic acid from water using mesoporous zeolitic imidazolate framework-8. *Chem. Eng. J.* 267, 9–15. <https://doi.org/10.1016/j.cej.2014.12.093>.
- Katheresan, V., Kansedo, J., Lau, S.Y., 2018. Efficiency of various recent wastewater dye removal methods: a review. *J. Environ. Chem. Eng.* 6, 4676–4697.
- Klett, C., Barry, A., Balti, I., Lelli, P., Schoenstein, F., Jouini, N., 2014. Nickel doped Zinc oxide as a potential sorbent for decolorization of specific dyes, methylorange and tartrazine by adsorption process. *J. Environ. Chem. Eng.* 2, 914–926. <https://doi.org/10.1016/j.jece.2014.03.001>.

- Konnerth, H., Matsagar, B.M., Chen, S.S., Precht, M.H.G., Shieh, F.-K., Wu, K.C.-W., 2020. Metal-organic framework (MOF)-derived catalysts for fine chemical production. *Coord. Chem. Rev.* 416, 213319. <https://doi.org/10.1016/j.ccr.2020.213319>.
- Konno, H., Nakasaka, Y., Yasuda, K., Omata, M., Masuda, T., 2020. Surfactant-assisted synthesis of nanocrystalline zeolitic imidazolate framework 8 and 67 for adsorptive removal of perfluorooctane sulfonate from aqueous solution. *Catal. Today Spec. Issue 17th Korea-Jpn. Symp. Catal.* 352, 220–226. <https://doi.org/10.1016/j.cattod.2019.12.036>.
- Kumar, K.V., 2006. Linear and non-linear regression analysis for the sorption kinetics of methylene blue onto activated carbon. *J. Hazard. Mater.* 137, 1538–1544.
- Kundu, S., Chowdhury, I.H., Naskar, M.K., 2017. Synthesis of hexagonal shaped nanoporous carbon for efficient adsorption of methyl orange dye. *J. Mol. Liq.* 234, 417–423. <https://doi.org/10.1016/j.molliq.2017.03.090>.
- Lee, C., Chen, C., Liao, Y., Wu, K.C., Chueh, C., 2019. Enhancing efficiency and stability of photovoltaic cells by using perovskite/Zr-MOF heterojunction including bilayer and hybrid structures. *Adv. Sci.* 6, 1801715.
- Li, J., Wu, Z., Duan, Q., Alsaedi, A., Hayat, T., Chen, C., 2018a. Decoration of ZIF-8 on polypyrrole nanotubes for highly efficient and selective capture of U (VI). *J. Clean. Prod.* 204, 896–905.
- Li, N., Zhou, L., Jin, X., Owens, G., Chen, Z., 2019. Simultaneous removal of tetracycline and oxytetracycline antibiotics from wastewater using a ZIF-8 metal-organic-framework. *J. Hazard. Mater.* 366, 563–572.
- Li, S., Chen, Y., Pei, X., Zhang, S., Feng, X., Zhou, J., Wang, B., 2016a. Water purification: adsorption over metal-organic frameworks. *Chin. J. Chem.* 34, 175–185. <https://doi.org/10.1002/cjoc.201500761>.
- Li, T., Zhang, Weiming, Zhai, S., Gao, G., Ding, J., Zhang, Wenbin, Liu, Y., Zhao, X., Pan, B., Lv, L., 2018b. Efficient removal of nickel (II) from high salinity wastewater by a novel PAA/ZIF-8/PVDF hybrid ultrafiltration membrane. *Water Res.* 143, 87–98.
- Li, Y., Zhou, K., He, M., Yao, J., 2016b. Synthesis of ZIF-8 and ZIF-67 using mixed-base and their dye adsorption. *Microporous Mesoporous Mater.* 234, 287–292. <https://doi.org/10.1016/j.micromeso.2016.07.039>.
- Liao, Y.-T., Matsagar, B.M., Wu, K.C.-W., 2018. Metal-organic framework (MOF)-derived effective solid catalysts for valorization of lignocellulosic biomass. *ACS Sustain. Chem. Eng.* 6, 13628–13643. <https://doi.org/10.1021/acssuschemeng.8b03683>.
- Liao, Y.-T., Nguyen, V.C., Ishiguro, N., Young, A.P., Tsung, C.-K., Wu, K.C.-W., 2020. Engineering a homogeneous alloy-oxide interface derived from metal-organic frameworks for selective oxidation of 5-hydroxymethylfurfural to 2,5-furandicarboxylic acid. *Appl. Catal. B Environ.* 270, 118805. <https://doi.org/10.1016/j.apcatb.2020.118805>.
- Lima, E.C., Hosseini-Bandegharai, A., Moreno-Piraján, J.C., Anastopoulos, I., 2019. A critical review of the estimation of the thermodynamic parameters on adsorption equilibria. Wrong use of equilibrium constant in the Van't Hoof equation for calculation of thermodynamic parameters of adsorption. *J. Mol. Liq.* 273, 425–434. <https://doi.org/10.1016/j.molliq.2018.10.048>.
- Liu, D., Zhong, C., 2010. Characterization of lewis acid sites in metal-organic frameworks using density functional theory. *J. Phys. Chem. Lett.* 1, 97–101.
- Liu, K., Zhang, S., Hu, X., Zhang, K., Roy, A., Yu, G., 2015. Understanding the adsorption of PFOA on MIL-101(Cr)-based anionic-exchange metal-organic frameworks: comparing DFT calculations with aqueous sorption experiments. *Environ. Sci. Technol.* 49, 8657–8665. <https://doi.org/10.1021/acs.est.5b00802>.
- Liu, Q., Zhou, Yi, Lu, J., Zhou, Yanbo, 2020a. Novel cyclodextrin-based adsorbents for removing pollutants from wastewater: a critical review. *Chemosphere* 241, 125043.
- Liu, S., Wang, W., Cheng, Y., Yao, L., Han, H., Zhu, T., Liang, Y., Fu, J., 2020b. Methyl orange adsorption from aqueous solutions on 3D hierarchical PbS/ZnO microspheres. *J. Colloid Interface Sci.* 574, 410–420. <https://doi.org/10.1016/j.jcis.2020.04.057>.
- Mahmoodi, N.M., 2014. Dendrimer functionalized nanoarchitecture: Synthesis and binary system dye removal. *J. Taiwan Inst. Chem. Eng.* 45, 2008–2020. <https://doi.org/10.1016/j.jtice.2013.12.010>.
- Maneung, T., Liew, J., Dai, Y., Kawi, S., Chong, C., Wang, C.-H., 2016. Activated carbon derived from carbon residue from biomass gasification and its application for dye adsorption: Kinetics, isotherms and thermodynamic studies. *Bioresour. Technol.* 200, 350–359. <https://doi.org/10.1016/j.biortech.2015.10.047>.
- Mathurasa, L., Damrongsiri, S., 2018. Low cost and easy rice husk modification to efficiently enhance ammonium and nitrate adsorption. *Int. J. Recycl. Org. Waste Agric.* 7, 143–151. <https://doi.org/10.1007/s40093-018-0200-3>.
- Doherty, C.M., Knystautas, E., Buso, D., Villanova, L., Konstas, K., Hill, A.J., Takahashi, M., Falcaro, P., 2012. Magnetic framework composites for polycyclic aromatic hydrocarbon sequestration. *J. Mater. Chem.* 22, 11470–11474. <https://doi.org/10.1039/C2JM31798B>.
- Mehmandoust, M.R., Motakef-Kazemi, N., Ashouri, F., 2019. Nitrate adsorption from aqueous solution by metal-organic framework MOF-5. *Iran. J. Sci. Technol. Trans. Sci.* 43, 443–449.
- Mohd Tahir, M.H., Teo, S.E., Moh, P.Y., 2017. Removal of methylene blue by iron terephthalate metal-organic framework/polyacrylonitrile membrane. *Trans. Sci. Technol.* 4, 14–21.
- Mokhtari, P., Ghaedi, M., Dashtian, K., Rahimi, M., Purkait, M., 2016. Removal of methyl orange by copper sulfide nanoparticles loaded activated carbon: kinetic and isotherm investigation. *J. Mol. Liq.* 219, 299–305.
- Nasser Abdelhamid, H., Zou, X., 2018. Template-free and room temperature synthesis of hierarchical porous zeolitic imidazolate framework nanoparticles and their dye and CO₂ sorption. *Green Chem.* 20, 1074–1084. <https://doi.org/10.1039/C7GC03805D>.
- Ohkubo, Y., Saito, T., Murakami, Y., Yokoyama, A., Kawase, Y., 2002. *Acta Crystallogr., Sect. A: Cryst. Phys., Diffr., Theor. Gen. Crystallogr. Acta Crystallogr., Sect. A: Cryst. Phys., Diffr., Theor. Gen. Crystallogr.* 32, 751–767, 1976. *Mater. Trans.* 43, 1469–1474.
- Omotunde, I., Okoronkwo, A., Oluwashina, O., 2018. Derived and thiourea-functionalized silica for cadmium removal: isotherm, kinetic and thermodynamic studies. *Appl. Water Sci.* 8, 21. <https://doi.org/10.1007/s13201-018-0652-7>.
- Park, K.S., Ni, Z., Côté, A.P., Choi, J.Y., Huang, R., Uribe-Romo, F. J., Chae, H.K., O'Keeffe, M., Yaghi, O.M., 2006. Exceptional chemical and thermal stability of zeolitic imidazolate frameworks. *Proc. Natl. Acad. Sci.* 103, 10186–10191. <https://doi.org/10.1073/pnas.0602439103>.
- Pavithra, K.G., Jaikumar, V., 2019. Removal of colorants from wastewater: a review on sources and treatment strategies. *J. Ind. Eng. Chem.* 75, 1–19.
- Phuong, V.T., Chokbunpiam, T., Fritzsche, S., Remsungnen, T., Rungrotmongkol, T., Chmelik, C., Caro, J., Hannongbua, S., 2016. Methane in zeolitic imidazolate framework ZIF-90: adsorption and diffusion by molecular dynamics and Gibbs ensemble Monte Carlo. *Microporous Mesoporous Mater.* 235, 69–77. <https://doi.org/10.1016/j.micromeso.2016.06.029>.
- Qi, X., Li, L., Tan, T., Chen, W., Smith Jr, R.L., 2013. Adsorption of 1-butyl-3-methylimidazolium chloride ionic liquid by functional carbon microspheres from hydrothermal carbonization of cellulose. *Environ. Sci. Technol.* 47, 2792–2798.
- Rahman, M., Sathasivam, K.V., 2015. Heavy metal adsorption onto *Kappaphycus* sp. from aqueous solutions: the use of error functions for validation of isotherm and kinetics models. *BioMed Res. Int.* 2015. <https://doi.org/10.1155/2015/126298>.
- Robati, D., Mirza, B., Rajabi, M., Moradi, O., Tyagi, I., Agarwal, S., Gupta, V.K., 2016. Removal of hazardous dyes-BR 12 and methyl orange using graphene oxide as an adsorbent from aqueous phase.

- Chem. Eng. J. 284, 687–697. <https://doi.org/10.1016/j.cej.2015.08.131>.
- Rodríguez-Carvajal, J., 2001. An introduction to the program FullProf 2000. Version July 54.
- Ryan, P., Konstantinov, I., Snurr, R.Q., Broadbelt, L.J., 2012. DFT investigation of hydroperoxide decomposition over copper and cobalt sites within metal-organic frameworks. *J. Catal.* 286, 95–102.
- Sapnik, A.F., Geddes, H.S., Reynolds, E.M., Yeung, H.H.-M., Goodwin, A.L., 2018. Compositional inhomogeneity and tuneable thermal expansion in mixed-metal ZIF-8 analogues. *Chem. Commun.* 54, 9651–9654. <https://doi.org/10.1039/C8CC04172E>.
- Sirajudheen, P., Karthikeyan, P., Vigneshwaran, S., Meenakshi, S., 2020. Synthesis and characterization of La(III) supported carboxymethylcellulose-clay composite for toxic dyes removal: evaluation of adsorption kinetics, isotherms and thermodynamics. *Int. J. Biol. Macromol.* 161, 1117–1126. <https://doi.org/10.1016/j.ijbiomac.2020.06.103>.
- Siyal, A.A., Shamsuddin, M.R., Khan, M.I., Rabat, N.E., Zulfiqar, M., Man, Z., Siame, J., Azizli, K.A., 2018. A review on geopolymers as emerging materials for the adsorption of heavy metals and dyes. *J. Environ. Manage.* 224, 327–339. <https://doi.org/10.1016/j.jenvman.2018.07.046>.
- Sun, J., Semenchenko, L., Lim, W.T., Ballesteros Rivas, M.F., Varela-Guerrero, V., Jeong, H.-K., 2018. Facile synthesis of Cd-substituted zeolitic-imidazolate framework Cd-ZIF-8 and mixed-metal CdZn-ZIF-8. *Microporous Mesoporous Mater.* 264, 35–42. <https://doi.org/10.1016/j.micromeso.2017.12.032>.
- Tsai, C.-W., Kroon, R.E., Swart, H.C., Terblans, J.J., Harris, R.A., 2019. Photoluminescence of metal-imidazolate complexes with Cd (II), Zn(II), Co(II) and Ni(II) cation nodes and 2-methylimidazole organic linker. *J. Lumin.* 207, 454–459. <https://doi.org/10.1016/j.jlumin.2018.11.026>.
- Wang, J., Li, Y., Lv, Z., Xie, Y., Shu, J., Alsaedi, A., Hayat, T., Chen, C., 2019. Exploration of the adsorption performance and mechanism of zeolitic imidazolate framework-8@graphene oxide for Pb (II) and 1-naphthylamine from aqueous solution. *J. Colloid Interface Sci.* 542, 410–420. <https://doi.org/10.1016/j.jcis.2019.02.039>.
- Wang, Y., Zhao, W., Qi, Z., Zhang, L., Zhang, Y., Huang, H., Peng, Y., 2020. Designing ZIF-8/hydroxylated MWCNT nanocomposites for phosphate adsorption from water: capability and mechanism. *Chem. Eng. J.* 394, 124992. <https://doi.org/10.1016/j.cej.2020.124992>.
- Wong, Y., Szeto, Y., Cheung, W., McKay, G., 2004. Pseudo-first-order kinetic studies of the sorption of acid dyes onto chitosan. *J. Appl. Polym. Sci.* 92, 1633–1645.
- Wu, Y., Xie, Y., Zhong, F., Gao, J., Yao, J., 2020. Fabrication of bimetallic Hofmann-type metal-organic Frameworks@ Cellulose aerogels for efficient iodine capture. *Microporous Mesoporous Mater.* 306, 110386.
- Xu, W., Chen, H., Jie, K., Yang, Z., Li, T., Dai, S., 2019. Entropy-driven mechanochemical synthesis of polymetallic zeolitic imidazolate frameworks for CO₂ fixation. *Angew. Chem.* 131, 5072–5076. <https://doi.org/10.1002/ange.201900787>.
- Yaghi, O.M., O’Keeffe, M., Ockwig, N.W., Chae, H.K., Eddaoudi, M., Kim, J., 2003. Reticular synthesis and the design of new materials. *Nature* 423, 705–714.
- Yang, Y., Yang, J., Du, Y., Li, C., Wei, K., Lu, J., Chen, W., Yang, L., 2019. Preparation and characterization of cationic water-soluble pillar[5]arene-modified zeolite for adsorption of methyl orange. *ACS Omega* 4, 17741–17751. <https://doi.org/10.1021/acsomega.9b02180>.
- Yu, J., Zhang, X., Wang, D., Li, P., 2018. Adsorption of methyl orange dye onto biochar adsorbent prepared from chicken manure. *Water Sci. Technol.* 77, 1303–1312.
- Zhang, X., Qian, L., Yang, S., Peng, Y., Xiong, B., Li, J., Fang, P., He, C., 2020. Comparative studies of methyl orange adsorption in various metal-organic frameworks by nitrogen adsorption and positron annihilation lifetime spectroscopy. *Microporous Mesoporous Mater.* 296, 109993.
- Zhou, Yanbo, Lu, J., Zhou, Yi, Liu, Y., 2019. Recent advances for dyes removal using novel adsorbents: a review. *Environ. Pollut.* 252, 352–365.
- Zhu, K., Chen, C., Xu, H., Gao, Y., Tan, X., Alsaedi, A., Hayat, T., 2017. Cr(VI) reduction and immobilization by core-double-shell structured magnetic polydopamine@zeolitic idazolate frameworks-8 microspheres. *ACS Sustain. Chem. Eng.* 5, 6795–6802. <https://doi.org/10.1021/acssuschemeng.7b01036>.